ESAIM: PROCEEDINGS, Juillet 2013, Vol. 40, p. 16-33
C. Bourdarias, S. Gerbi, Editors

DROP PINCH-OFF FOR DISCRETE FLOWS FROM A CAPILLARY *, **

F. Bierbrauer[1], N. Kapur[2] and M.C.T. Wilson[2]

Abstract. The problem of drop formation and pinch-off from a capillary tube under the influence of gravity has been extensively studied when the internal capillary pressure gradient is constant. This ensures a continuous time independent flow field inside the capillary tube typically of the Poiseuille flow type. Characteristic drop ejection behaviour includes: periodic drop ejection, drop ejection with associated satellite production, complex dripping, chaotic behaviour and jetting. It is well known that this characteristic behaviour is governed by the Weber (We) and Ohnesorge (Oh) numbers (for a given Bond number) and may be delineated in a We verses Oh operability diagram.
An in-depth physical understanding of drop ejection is also of great importance to industry where the tight control of drop size and ejection velocity are of critical importance in industrial processes such as sealants used in electronics assembly and inkjet printing. However, the use of such a continuous flow approach for drop ejection in industry is often impractical since such flows cannot be operator controlled. For this reason it is important to investigate so-called discrete pipe flows where the flow can be turned on and off at will. This means the flow inside the pipe is now time-dependent being controlled in a step-wise fashion.
As a first stage in the investigation of drop pinch-off behaviour in discrete pipe flows this paper will study the critical pinch-off time required for drop ejection starting from a pendant drop. This is the discrete amount of time the pipe flow is turned on for in order for a drop to be ejected from the capillary. A Newtonian incompressible free-surface CFD flow code developed at the University of Leeds is used to investigate the critical pinch-off time for a range of internal pipe velocities (the central flow maximum in Poiseuille flow). It is found that the time required for drop ejection to occur decreases exponentially with internal pipe velocity. These characteristic times are also far smaller than typical static drop release times expected from Harkins and Brown analyses. The phenomenology of the process is due to the creation of a capillary wave at the pipe exit upon the sudden turning on of the flow inside the pipe. The capillary wave acts to transport fluid from the upper part of the forming pendant drop at the end of the capillary to the lower part of the drop both lowering the pendant drop centre-of-mass and thinning the neck region connecting the drop to the pipe. This allows the drop to be pinched off at an earlier than expected time as compared to static drop release times.

1. Introduction

The ejection of drops from a capillary plays an important role in engineering and industry. Typical examples include spray painting of car door panels, water-spray cooling in the steel industry, sealants used in electronics

* *The authors wish to thank the Technology Strategy Board for funding under Grant no. TS/H001166/1*

** *The authors appreciate the use of the finite element free surface code developed by Oliver Harlen of the School of Mathematics, University of Leeds*

[1] School of Computing, Mathematics and Digital Technology, Manchester Metropolitan University, Manchester, M1 5GD, UK

[2] School of Mechanical Engineering, University of Leeds, Leeds, LS2 9JT, UK

assembly and more recently in ink-jet printing. Such systems are constituted by a capillary or spray nozzle attached to a pipe which provides a given liquid under pressure. The fluid is forced through the pipe so that, at the open end, a pendant drop starts to form (the drop formation stage); this grows until the forces at work detach the drop whether through drop ejection due to inertia or drop release due to gravitational forces (the drop ejection stage). The drop formation stage involves the growth of a pendant drop at the end of the capillary which forms with a moving interface or free surface.

For the simplified case of free-surface flows where the external environment outside of the drop liquid is assumed to be a passive gas at constant pressure (or of density significantly less than the drop fluid) we have the situation shown in Figure 1. In this paper we study the process of ejecting a drop of incompressible Newtonian

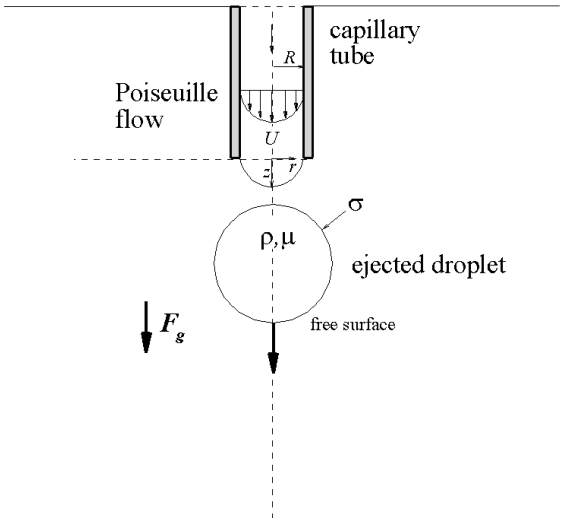

FIGURE 1. Drop ejection parameters and fluid dynamical scales.

liquid, of density ρ, viscosity μ and surface tension σ, from a capillary tube under the influence of gravity. As seen in Figure 1 the capillary is oriented vertically down in the same direction as the force of gravity $\mathbf{F}_g$. The capillary tube itself acts to define a natural set of flow parameters including the tube radius R, the central flow velocity U within the pipe as well as the flow rate Q. The developed flow itself is assumed axisymmetric and the typical flow field within the capillary may be expressed in cylindrical polar coordinates (r, z). The flow is generally axisymmetric so that the flow velocity components (u_r, u_z), radial and axial components, within the pipe are given by

$$u_r = 0, \qquad u_z(r) = \frac{U}{R^2}(R^2 - r^2), \qquad U = -\frac{R^2}{4\mu}\left(\frac{\Delta p}{\Delta z}\right) \tag{1}$$

This is the well known Poiseuille flow in a pipe with the velocity scale U defined in terms of the pressure gradient within the pipe. This *pipe flow velocity* scale is also the maximum velocity along the symmetry line of the flow. The pressure gradient acts to "push" the fluid out of the pipe. Fluid within the pipe is acted on by various forces including inertia, the pressure gradient, gravity (with acceleration $g = 9.81$ m/s^2), internal frictional forces or viscosity and, once a free surface has formed at the end of the pipe, the surface tension force which acts on the fluid boundary to lower surface energy and restore drop equilibrium. The physical scales of the flow are then the length scale R, velocity scale U, advective time scale $T_{adv} = R/U$ as well as a natural pressure scale ρU^2. These scales typically characterise the non-dimensional fluid parameters such as the Weber number $We = \rho R U^2/\sigma$ (the ratio of inertial to surface tension forces), the Reynolds number $Re = \rho R U/\mu$ (the ratio of inertial to viscous forces) and the Froude number $Fr = U^2/gR$ (the ratio of inertial to gravitational forces). A related set of parameters can be defined through the Ohnesorge number $Oh = \sqrt{We}/Re = \mu/\sqrt{\rho R \sigma}$

which measures the ratio of viscous to inertial and surface forces, the Bond number $Bo = \rho g R^2/\sigma$ (the ratio of gravitational to surface tension forces) and the Capillary number $Ca = \mu U/\sigma$(the ratio of viscous to surface tension forces).

1.1. **Drop Formation from a Capillary**

The best known case of drop ejection from a capillary are the dripping faucet experiments used to demonstrate the possibility of chaotic behaviour in drops of water dripping from a tap [1]. In these experiments a constant pressure gradient was applied within the capillary ensuring a continuous flow and subsequent drop formation and ejection from the pipe. We designate this type of flow within the capillary as time-independent *continuous* pipe flow. The dynamics of drop formation from such systems have been extensively studied over many years, focusing on jet break-up [2–4] and continuous dripping [1,5,6], and extending into related flows such as co-flowing liquid-liquid systems [7] and dispensing of complex fluids [8].

In investigating the measurement of surface tension, Harkins and Brown [9] conducted an extensive set of drop formation experiments to determine the critical drop masses/volumes when the pressure gradient is constant in the pipe but at very low pipe flow velocities. In this way it was hoped to obtain the critical drop volume required for a drop to be detached from the capillary. In this sense the drop was released rather than ejected as inertial forces were considered negligible.

Under stable conditions, continuous pipe flows can generate a reliable source of drops of a given volume and ejection speed. However, the drop formation and ejection process cannot be operator controlled. In the industrial application mentioned above, it would be beneficial to be able to eject droplets of a given volume at will. Note that the idea of producing drops on demand is well established in the widely studied context of inkjet printing, see e.g. [10–12]. There a pressure pulse, generated for example by a piezoelectric transducer, causes the ejection of a droplet from a nozzle. Since inkjet nozzles and droplets are so small, gravity plays a negligible role in the droplet formation and hence such flows belong to a different class from the pulsed capillary flows under gravity considered here.

Here, a modification of the continuous pipe flow defined previously in equation (1) is proposed so that the flow may be turned on and off when required. This makes the flow time dependent although still incompressible. The key assumption in the analysis presented here is that the flow in the capillary always has a fully developed radial profile, whose amplitude varies with time. Hence the previously defined axial flow which is a continuous flow is now modified into a step-wise *discrete* flow defined by altering the axial flow to become: $u_z(r,t) = \phi(r)\tau(t)$, where $\tau(t)$ is the time dependent component of the flow and $\phi(r)$ the space dependent Poiseuille flow component. Whereas the continuous pipe flow solution (1) is a solution of the Navier-Stokes equations in a cylindrical pipe of infinite length we propose a time dependent pipe flow where this new discrete condition for the axial flow is imposed only at the pipe inlet (see also Figure 7(b)). The difference between continuous and discrete flows is shown in Figure 2. The figure shows that the continuous case Figure 2(a) possesses a time dependent component with $\tau(t) = 1$ whereas the discrete case Figure 2(b) considers a time dependence where the flow is turned on and off in a discontinuous fashion.

2. Continuous Pipe Flow

Figure 3[1] shows photographs taken at 60 micro-second intervals (with time increasing left to right) of an experiment by Peregrine and co-workers [13] for water dripping from a glass capillary of radius 2.6 mm with a constant pressure gradient within the pipe. It demonstrates the typical process of drop formation and dripping from a capillary for the continuous case. These experimental results are for water dripping from the end of a glass capillary of radius 2.6 mm taken at 60 micro-second intervals. The residual fluid remaining behind from a previous drop ejection starts to grow into a larger pendant drop still attached to the capillary exit, see the first image on the left of Figure 3. Fluid continues to flow into the pendant drop which expands downward

[1]Reprinted with permission from [Peregrine, D.H., Shoker, G., Symon, A., J. Fluid Mech., 212:25–39, 1990.]. Copyright [1990], Cambridge University Press.

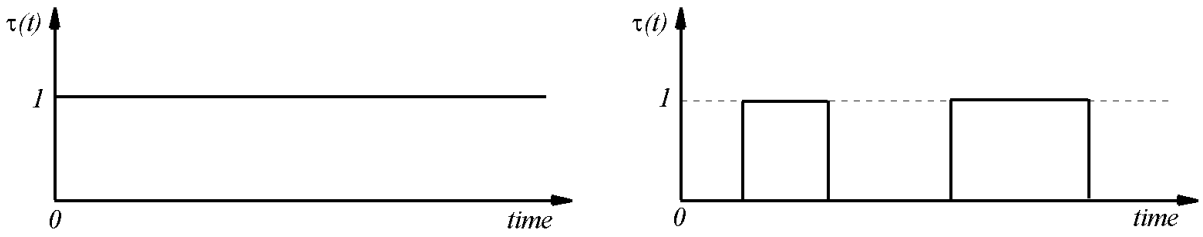

FIGURE 2. Plots of the time dependent part of the internal pipe flow $\tau(t)$ for (a) a typical continuous process with a constant time dependent component and (b) a simple discrete process with a discontinuous time dependent component.

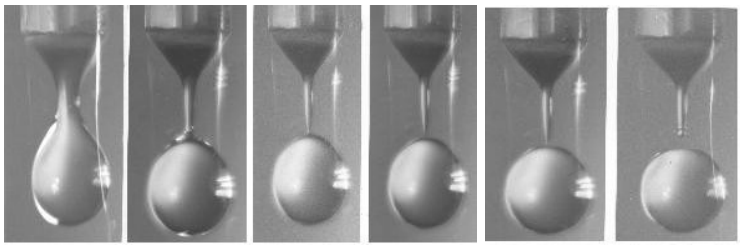

FIGURE 3. Typical drop formation, pinch-off and ejection at the open end of a capillary (the top of each photo indicates the exit nozzle of the capillary, gravity is oriented vertically downwards) [13].

under the influence of gravity and inertia, second image in Figure 3. The drop starts to elongate and the neck region attaching the drop to the capillary starts to thin out (necking), third image in Figure 3. This neck forms a thread which creates a bridge between a cone-like region near the capillary exit and the top of the primary drop (threading), the fourth and fifth images in Figure 3. Eventually the pendant drop pinches off at the end of the thread (last image in Figure 3), forming the primary ejected drop, while the thread recoils towards the residual fluid attached to the capillary exit (pinch-off). This describes the basic drop ejection phenomenon for the continuous process, although the thread may also detach from the cone-like residual fluid at the capillary exit. This creates a freely moving thread which recoils in opposite directions so that a satellite drop can form. This satellite may rejoin the residual fluid, join the primary ejecting drop or remain separate.

2.1. **Dripping Modes**

Drop formation depends on the balance of forces acting on the fluid which may be delineated within a so-called operability diagram of Ohnesorge verses Weber number at constant Bond number. These parameters describe the relative sizes of inertia to surface tension forces (We) and viscous to surface tension and inertial forces (Oh) while the ratio of gravitational to surface tension forces is constant (Bo). This is shown in Figure 4[2] for $Bo = 0.3$ from a study by Subramani *et al* [1].

The operability diagram is clearly separated into various distinct regions including a triangular region, indicated by the designation P1 ($0.005 < Oh < 3$, $0.1 < We < 1.1$), where drops are ejected in a periodic fashion with equal ejection times, this is called period one dripping. Underneath this region, indicated as P1S ($0.005 < Oh < 3$, $We < 0.1$) period one dripping occurs with the associated creation of a satellite drop. To the left and above the P1 region ($0.001 < Oh < 0.4$, $We > 0.1$) the drops are still ejected periodically although

[2]Reprinted with permission from [Subramani H.J., Yeoh H.-K., Suryo R., Xu Q., Ambravaneswaran B., Basaran O., Phys. Fluids, 18:032106-1032106-13, 2006]. Copyright [2006], American Institute of Physics.

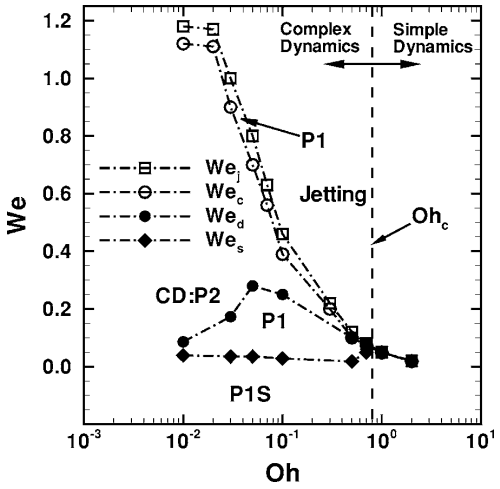

FIGURE 4. Operability diagram for the continuous process showing dripping modes for $Bo = 0.3$ resized for the non-dimensional parameters used in this paper [1].

undergo period doubling, e.g. P2 dripping where two types of drops of unequal size and ejection times are ejected, this eventually becomes complex dripping (CD) and finally chaotic dripping. Towards the right and above the P1 region of the diagram ($0.01 < Oh < 10$, $We > 0.1$) the drops are ejected as a jet (J). there is also a very thin P1 region trapped between the CD and jetting regions. The various critical values We_j, We_s indicate the transition between the regions.

2.2. **Static Pinch-Off Behaviour**

For very small pipe flow velocities (small We) where the fluid flows slowly into the growing pendant drop, the drop undergoes so-called static pinch-off behaviour. The drop grows slowly until the gravitational and surface tension forces balance, and the drop will be released once this threshold is exceeded. This process was studied extensively by Harkins and Brown [9] where a drop must be pinched off whenever the total pendant drop volume (the volume of the the residual fluid plus the thread and the forming primary drop) exceeds a certain critical value V_c. For small pipe flow velocities, and ignoring the effects of viscosity, this is determined by a balance between gravitational buoyancy forces $F_B = V_c g \Delta\rho$ acting on the pendant drop mass and surface tension forces $F_S = 2\pi\sigma R$ attempting to minimise drop surface energy. The ejected drop volume V_d is then determined from

$$V_d = \frac{2F\pi\sigma R}{g\Delta\rho} \tag{2}$$

Where $F = V_d/V_c$ (≈ 0.6) is the so-called Harkins-Brown correction factor which compensates for the remaining residual fluid at the pipe exit after a drop has been ejected. We must emphasise that the original Harkins-Brown approach studied a static pinch-off situation meaning that the drop was released rather than ejected just when the gravitational force exceeded the surface tension force. This occurs in a static manner whereby no other forces other than the balance between gravity and surface tension act. That is, there is no flow within the pipe or the pendant drop. This corresponds to static pinch-off behaviour.

3. DISCRETE PIPE FLOWS

As mentioned earlier in Section 1.1, discrete pipe flow may be defined through the axial velocity component given in the form:

$$u_z(r,t) = \phi(r)\tau(t) \tag{3}$$

separated into space dependent $\phi(r)$ (Poiseuille flow) and time dependent $\tau(t)$ components respectively. Note that in reality any flow imposed at the inlet takes a given time to build up to the Poiseuille pipe flow which would imply that $\phi = \phi(r,t)$. However, for the purposes of simplicity and as a representation of a realistic limiting case the representation (3) will be used in this paper. The simplest type of discrete flow is one which undergoes a very rapid change in velocity for a given timescale T_D so that it is natural to express it in terms of the Heaviside function:

$$H(t) = \begin{cases} 1 & \text{if} \quad t \geq 0 \\ 0 & \text{if} \quad t < 0 \end{cases}$$

where the flow is turned on as a square wave pulse or step-wise flow. This may then be expressed with $\phi(r) = U(R^2 - r^2)/R^2$ and $\tau(t) = H(T_D - t)$ so that:

$$u_z(r,t) = \phi(r)\tau(t) = \frac{U}{R^2}(R^2 - r^2)H(T_D - t) = \begin{cases} \frac{U}{R^2}(R^2 - r^2) & \text{if} \quad t \leq T_D \\ 0 & \text{if} \quad t > T_D \end{cases} \tag{4}$$

Note that once we have defined the discrete flow in this way it becomes possible to express the discrete volume

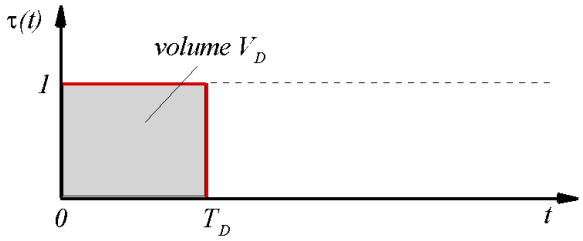

FIGURE 5. Diagram showing a typical step-wise time dependent component of discrete pipe flow axial velocity over a discrete time T_D and delivering an implied discrete volume $V_D = \pi R^2 U T_D/2$

delivered within the pipe over time T_D as (see Figure 5):

$$V_D = 2\pi \int_0^R \int_0^{T_D} u_z(r,t)\, drdt = \frac{2\pi U}{R^2} \int_0^R \int_0^{T_D} (R^2 - r^2)H(T_D - t)\, drdt = \frac{1}{2}\pi R^2 U T_D \tag{5}$$

The step-wise structure of the time dependent component $\tau(t)$ is shown diagrammatically in Figure 5.

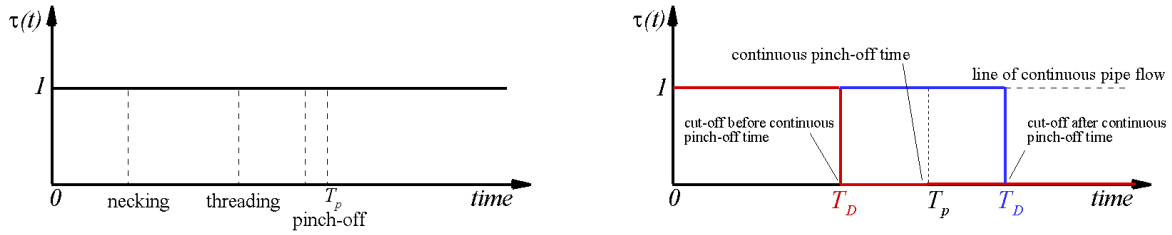

FIGURE 6. Comparison of (a) the continuous case indicating the characteristic drop formation stages of necking, threading and pinch-off with characteristic pinch-off timescale T_p, with (b) the discrete case showing flow discontinuity with characteristic timescale T_D shorter (red) and longer (blue) than the continuous timescale T_p.

The time dependent component $\tau(t)$ of the continuous and discrete flows may be compared by considering the drop formation and ejection process for the continuous case. Figure 6(a) shows the typical course of events in continuous drop formation and ejection including: necking, threading and pinch-off indicating the characteristic pinch-off timescale as T_p. As a comparison Figure 6(b) shows the discrete case where the flow has been shut off at time $T_D < T_p$ before (red) and after (blue), $T_D > T_p$, the continuous pinch-off time.

4. Mathematical Modelling

In this paper we make use of a finite element (FE) numerical model for free surface flows developed in the School of Mathematics at the University of Leeds by Oliver Harlen and Neil Morrison and further modified by the authors where necessary for the problem under consideration. The model was first developed for Newtonian incompressible fluids although later extended for particular non-Newtonian models. Details of the model are to be found in [14]. It is a Lagrangian-Eulerian finite element code where the stress in each mesh element is computed in a Lagrangian manner combined with an Eulerian computation of the discrete nodal velocities and pressures at each time step. The mesh itself is Lagrangian so that the nodes move with the flow. This makes it ideal for a constantly changing flow such as a free surface flow although it suffers from the well known problem of mesh distortion as the flow undergoes high shear. For this reason remeshing is necessary as well as the introduction of extra mesh nodes to maintain resolution in depleted regions and the removal of nodes in congested regions [15].

The method has been validated for free-surface flows such as those involved in inkjet printing where a drop is ejected from a nozzle [16]. Since this involves the pinching off of fluid elements when the drop is ejected from the pipe, it requires an extra condition so the numerical model "knows" when to pinch off the drop as the connecting thread (see the endpoint of the thread connecting the pendant drop to the primary in the last photo of Figure 3) thins beyond the limit of resolution. In the model the pinch-off condition is enforced once the minimum neck radius is below the cut-off threshold of less than 1% of the pipe exit radius. At this point, the mesh is severed along the shortest edge such that two separate meshes are created - one for the drop and one for the residual liquid.

One way to further test the model is to study the continuous drop formation process especially the dripping modes shown in Figure 4. This would confirm its use when studying the drop formation process including the discrete case.

4.1. Governing Equations and Boundary Conditions

In order to study the drop formation process we choose to model the process by modelling both the flow inside the capillary, of radius R, up to a distance h above the pipe exit and the flow that forms once the pendant drop grows, see Figure 7(a). Figure 7 shows the region of the pipe $0 \leq z \leq h$ that is being modelled as well as the region of the forming pendant drop and its free bounday. The fluid inside the pipe is under the influence of a pressure gradient which forces fluid out of the pipe exit. In addition, gravity acts in the negative z direction to further "pull" on the forming pendant drop.

The non-dimensionalised Navier-Stokes equations, using the scales stated in Section 1: lengthscale R, velocity scale U, timescale R/U, pressure scale ρU^2, may then be summarised as follows, see also Figure 7:

$$\frac{\partial \mathbf{u}}{\partial t} + (\mathbf{u}.\nabla\mathbf{u}).\mathbf{u} = -\nabla p + \frac{1}{Re}\nabla^2\mathbf{u} - \frac{\mathbf{k}}{Fr}, \qquad \nabla \cdot \mathbf{u} = 0 \qquad \text{in} \qquad \Omega, t > 0 \tag{6}$$

This is defined inside a domain $\Omega = \Omega_p \cup \Omega_{FS}$ where $\Omega_p = \{(r,z) : -R < r < R, 0 \leq z < h\}$ represents the pipe (p) and $\Omega_{FS} = \{(r,z) : f(r,z,t) < 0\}$ the free surface (FS) with boundaries $\partial\Omega = \partial\Omega_{in} \cup \partial\Omega_w \cup \partial\Omega_{FS}$ where $\partial\Omega_w = \{(r,z) : r = \pm R, 0 \leq z \leq h\}$, $\partial\Omega_{in} = \{(r,z) : z = h, -R \leq r \leq R\}$ and $\partial\Omega_{FS} = \{(r,z) : f(r,z,t) = 0\}$ where $f(r,z,t) = 0$ defines the free surface. The vector $\mathbf{k}$ is a unit vector in the z direction. Here the size of gravitational forces in comparison with inertia is taken into account by the Froude number, $Fr = U^2/gR$, and viscous forces by the Reynolds number, $Re = \rho UR/\mu$, see equation (6).

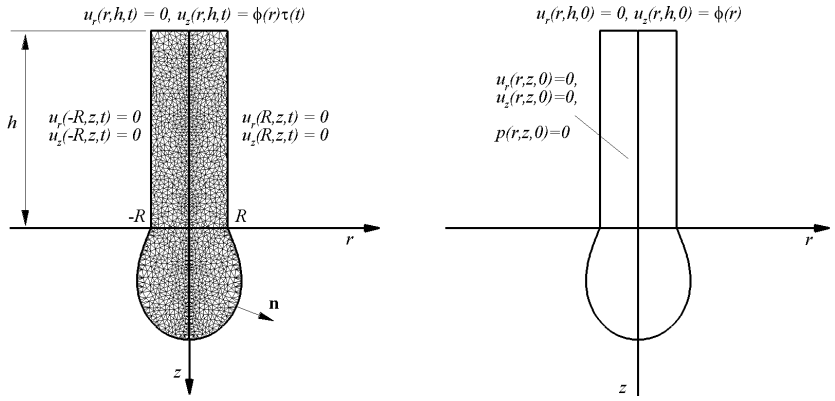

FIGURE 7. Diagram showing (a) the finite element mesh, boundary conditions and (b) initial conditions for the discrete flow problem studied in this paper.

This is subject to wall conditions along the pipe wall at $r = \pm R$:

$$\mathbf{u}(-R, z, t) = \mathbf{0}, \qquad \mathbf{u}(R, z, t) = \mathbf{0} \qquad \text{on} \qquad \partial\Omega_w, t > 0 \tag{7}$$

and a discrete inlet condition, at $z = h$, defined for a time T_D in equation (4) and shown in Figure 5:

$$\mathbf{u}(r, h, t) = (u_r(r, h, t), u_z(r, h, t))^T = \begin{cases} (0, \phi(r))^T & \text{for} \quad 0 < t \leq T_D \\ (0, 0)^T & \text{for} \quad t > T_D \end{cases}, \qquad \text{on} \qquad \partial\Omega_{in} \tag{8}$$

Note that this condition defined by the decomposition (4) is only imposed along the inlet at $z = h$. The free surface (FS) boundary condition along the free surface of the forming drop (κ the curvature and $\mathbf{n}$ a unit normal vector to the free surface) obeys the equality between the normal stress and capillary forces (here indicated by the Weber number and surface curvature):

$$\mathbf{n} \cdot \left[-p\mathbf{I} + \frac{1}{Re}(\nabla\mathbf{u} + \nabla\mathbf{u}^T) \right]_{FS} = \frac{\kappa\mathbf{n}}{We}, \qquad \text{on} \qquad \partial\Omega_{FS}, t > 0 \tag{9}$$

and an initial condition at $t = 0$, which is consistent with the boundary conditions stated in (7) and (8), see Figure 7(b):

$$\mathbf{u}(r, z, 0) = \mathbf{0}, \qquad p(r, z, 0) = 0 \qquad \text{in} \qquad \Omega \tag{10}$$

$$\mathbf{u}(r, h, 0) = (0, \phi(r))^T \qquad \text{on} \qquad \partial\Omega_{in} \tag{11}$$

In this paper the formation of drops, through the addition of a quantity of fluid to an existing pendant drop hanging from the end of the capillary, is investigated. The initial condition for the free surface shape therefore requires careful construction, by the process described in the next section.

4.2. **Building a Pendant Drop**

As a first stage in the modelling of the drop formation process we are able to build a pendant drop at the end of the capillary which will form the initial condition for the drop formation process. Starting from the state where no liquid hangs below the capillary, see Figure 8 we may then build a pendant drop of any volume we require. The flow is turned on as a square wave pulse, see Figure 5, for a time $T_{pend} = 2V_{pend}/\pi R^2 U$ where the volume V_{pend} is a pre-chosen pendant drop volume.

Figure 8 shows contours of the (magnitude of) velocity inside the capillary and the forming pendant drop. Note the blue colour indicating small velocities near the pipe walls and a red colouring for the largest velocity

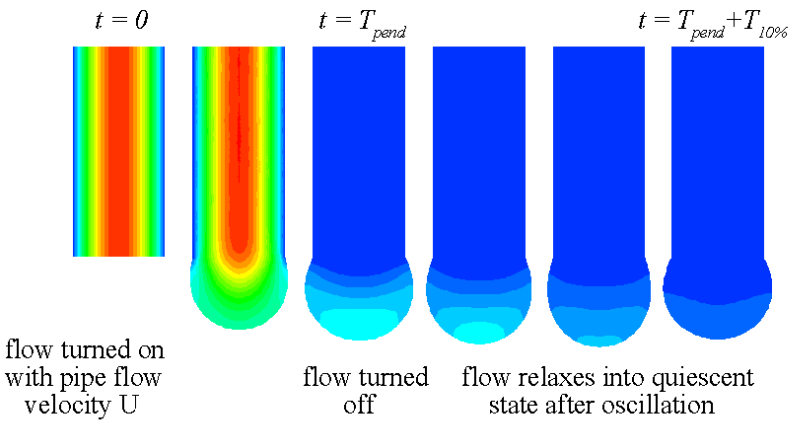

FIGURE 8. Building a pendant drop from the "zero" initial condition over a time T_{pend} of volume V_{pend} followed by the decay of oscillations induced at the end of the building process.

at the centre of the (Poiseuille) flow. This is clearly seen in Figure 8 where the flow velocity is shown to grow a drop at the end of the capillary (the second plot from the left), after which the flow is turned off here marked by the time $t = T_{pend}$.

This discrete time $T_D = T_{pend}$ varies depending on the internal pipe velocity U that is used while the flow is turned on. The only requirement is that the volume of the pendant drop that is built up is smaller than the critical break off volume V_d for a static drop, see equation (2). In this paper we chose to use a value of V_{pend} close to but smaller than the static break off volume V_d. At the conclusion of this drop building process we add on an extra amount of time in order to dissipate any remaining drop oscillations from the building process, see the last three plots in Figure 8. This amount of time may be calculated since it is known [17] that a pendant drop oscillates with frequency given by $f_{osc} = \sqrt{8\sigma/3\pi\rho V_{pend}}$ and that the decay rate τ_d of the oscillation varies with f_{osc}, V_{pend} and kinematic viscosity ν as follows $\tau_d = V_{pend}^{1/3}/\sqrt{2\pi f_{osc}\nu}$. If the amplitude decay $A(t)$ is assumed to be given by $A(t) = A_0 e^{-\lambda t}$, where $\lambda = 1/\tau_d$, then the amplitude will decay to 10% of its initial value A_0 in a time of $T_{10\%} = -ln(0.1)/\lambda$. This means that the total time needed for the building of a pendant drop is $T_{pend} + T_{10\%}$, if we assume that 10% is sufficient for most of the oscillations to have died away. It was found that, for the cases studied in this paper, this amount of time was more than sufficient to dissipate extraneous oscillations.

4.3. **Ejecting a Drop**

Ordinarily (for example in the Harkins-Brown case), in order to eject a drop we must inject an additional volume, V_D ($D \equiv$ discrete volume), of fluid into the pipe so that the total volume, $V_{pend} + V_D$, attached to the capillary exit has a weight that exceeds the capillary forces necessary to support it. The total amount of fluid entering and leaving the pipe must be conserved (conservation of mass/volume). Therefore, conservation of volume implies:

$$V_{pend} + V_D = V_{drop} + (V_{sat}) + V_{res} \tag{12}$$

This is shown diagrammatically in Figure 9. Note that to make sure only a given volume V_D is added on we turn the flow on for a time $T_D = \pi R^2 U T_D/2$ as shown in Figure 5. Note also that this volume is controlled by the discrete time T_D at a given pipe velocity U. It is also clear from Figure 9 that it is possible for a satellite drop to be formed which is why a volume V_{sat} is shown in brackets in equation (12), although no satellite is shown in the figure. The occurrence of satellites during the drop formation process is not the subject of this

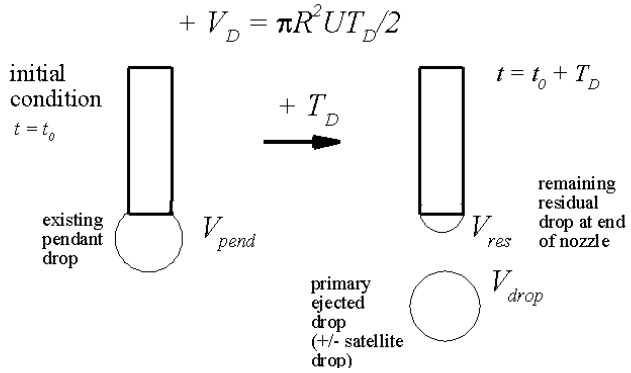

FIGURE 9. Diagrammatic process of drop ejection by adding a discrete volume V_D onto the existing pendant drop volume V_{pend} at $t = t_0$ to eject a drop of volume V_{drop} after a time $t = t_0 + T_D$.

paper and is left for an upcoming study. After ejection a residual volume V_{res} remains attached to the capillary exit.

4.4. **Code Validation**

The finite element code was previously used to study the inkjet printing process [15, 16]. It was validated against experimental results for both the continuous (CIJ) and drop-on-demand (DOD) modes used for inkjet printers. In the CIJ case ejected drop shapes and breakup compared extremely well to Laser Doppler anemometry experiments both qualitatively and quantitatively [15]. Similarly, for the DOD case the simulations were compared with flash photography agreeing well with drop formation at the pipe exit nozzle, pinch-off length, ejected drop shape and ejected drop tip position [16].

As an additional qualitative test of the code we study the continuous drop formation process within the range of scales required for this paper. For this reason we will investigate how the code performs when modelling the continuous process so that the characteristic dripping modes of Figure 4 may be demonstrated. This is the continuous case so that the discrete timescale of the problem defined in equations (7)-(11) has $T_D \to \infty$ with $\tau(t) = 1$. The regions to be studied in the operability diagram of Figure 4 are shown as green and orange dots in the figure. These correspond with the following Weber and Ohnesorge number pairs (Oh, We): the first set of plots correspond to the points $(0.03, 0.3)$, $(0.03, 0.6)$, $(0.03, 0.9)$ and the second to $(0.1, 1.2), (0.03, 0.1), (0.2, 0.3)$ at a Bond number of $Bo = 0.33$. We use the following fluid dynamical parameter values: $\rho = 1116$ kg/m^3, $\sigma = 0.044$ N/m, $R = 1.16$ mm for varying velocities U and viscosities μ. For example for $U = 0.1$ m/s and $\mu = 0.007$ Pas we find $We = 0.3$, $Re = 18.5$ and $Bo = 0.33$ giving $Oh = \sqrt{We}/Re = 0.03$.

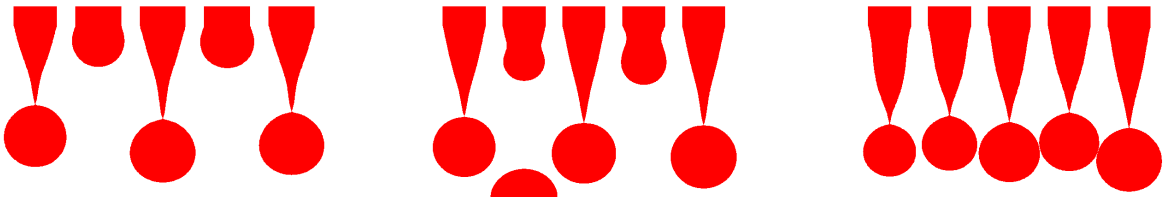

FIGURE 10. Plots of continuous drop formation and ejection for the case of (a) $(0.03, 0.3)$, (b) $(0.03, 0.6)$ and (c) $(0.03, 0.9)$.

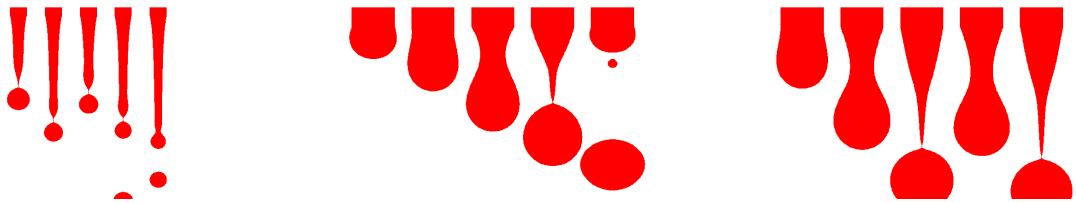

FIGURE 11. Plots of continuous drop formation and ejection for the case of (a) $(0.1, 1.2)$, (b) $(0.03, 0.1)$ and (c) $(0.2, 0.3)$

Figures 10 and 11 show plots of the drop outline as it grows and is ejected from the capillary. These points were chosen to correspond with varying kinds of drop formation and ejection. For example $(0.03, 0.9)$ corresponds to a relatively low Ohnesorge number and a high Weber number which means we expect little influence of viscosity on the pinch-off process but a strong tendency of the drop to restore itself to its equilibrium configuration due to high surface tension forces. We expect from Figure 4 that the process will be of the complex dripping type (most likely P2 period doubling) lying just outside the P1 triangle. We see immediately from Figure 10(c) that we get two sets of drops ejected at different pinch-off lengths and ejection times. For the case of $(0.03, 0.3)$ we expect P1 type behaviour and a single drop ejected regularly at equal times which is seen in Figure 10(a). The case of $(0.1, 1.2)$ is at a slightly larger Ohnesorge number so that viscous effects are more significant but are also at a quite large Weber number. We again expect complex dripping type behaviour but this time influenced by the larger viscosity which will tend to elongate a connecting thread between the capillary exit and the primary drop before pinching off. We can see this clearly in Figure 11(a). On the other hand the case of $(0.03, 0.1)$ represents smaller viscous forces and moderate sized surface forces and so we expect shorter threads than the previous case and from Figure 4 we expect to see satellite drops to be generated. This is easily observed in Figure 11(b). The simulation results clearly show good qualitative agreement with observed data. This shows how well suited this particular code is for the discrete case studied in the next section.

5. Critical Drop Ejection

This section will study the phenomenon of critical drop formation from a capillary in the case of discrete flows. To some degree this is akin to the static pinch-off phenomenon investigated by Harkins and Brown [9] and previously described in Section 2.2. However, in the discrete case, the flow is controlled by the discrete amount of time T_D for which fluid is injected into the pipe so that the ejection of a drop may occur or not depending on how long the flow is turned on for. It is expected that if the flow is not turned on long enough then the amount of fluid V_D added to the amount of fluid already present at the pipe exit V_{pend} will be below the critical amount needed to eject a drop (expressed in the Harkins-Brown sense). This means that the added fluid simply builds a bigger pendant drop which does not pinch-off. Similarly, if the flow is turned on beyond this proposed critical ejection time $T_D > T_{crit}$ then the drop will be ejected and also contribute to the building of a new residual drop at the pipe exit and/or eject another drop. We propose to study the critical ejection time that is just enough to eject a drop but no more. This means that if this time is even a little below the critical value then the drop will not be ejected. Note that this critical ejection time will be a function of the pipe flow velocity U so that $T_{crit} = T_{crit}(U)$ since a higher flow velocity will inject more fluid into the pipe over a smaller discrete flow time T_D than for a smaller pipe flow velocity over the same time (since $V_D = \pi R^2 U T_D/2$). An important question to be answered is: "Does the critical ejection time depend on the pipe flow velocity in a simple way?", this asks whether this time will in fact respond in a similar way to the static case.

5.1. **Injecting Fluid into the Capillary**

The following fluid dynamical parameters will be used for the study: $\rho = 1000$ kg/m^3, $\mu = 0.02386$ Pas, $\sigma = 0.044$ N/m, $R = 1.02$ mm. To keep the problem simple we choose to study this phenomenon by first obtaining the static release volume needed to eject a drop using the Harkins-Brown approach. This forms a basis for the ejection study. For the above fluid parameters the critical drop release volume is given by equation (2), with a value of $F = 0.6$ we obtain $V_d = 2F\pi\sigma R/g\Delta\rho = 1.44 \times 10^{-8}$ m$^3 \equiv 14.4$ μL. We choose $V_{pend} = 13$ μL so that this lies just below the static release volume and provides a test of how the time needed to eject a drop T_D changes as U is increased from a small value to larger values. The algorithm is as follows:

(1) Start with an existing pendant drop volume $V_{pend} = 13$ μL and a given pipe flow velocity $U = 0.05$ m/s
(2) Turn on the discrete flow for a time T_D restricted as follows:
   (a) test run a simulation for a time $T_D^{(1)}$ where a volume $V_D^{(1)}$ is injected into the pipe
   (b) if a drop is not ejected increase the time to $T_D^{(2)}$ in small amounts until a drop gets ejected
   (c) repeat this process until the difference between these two times (the drop not ejected T_D^{ne} and the drop ejected T_D^{ej}) $(T_D^{ej} - T_D^{ne})/T_D^{ej} \times 100 < 1\%$, choose this as the critical ejection time T_{crit}.
(3) increment the velocity in (1) by 0.05 m/s and repeat steps 2(a)-(c) to obtain the other critical ejection times T_{crit} as a function of U.

5.1.1. *Critical Drop Ejection Time*

Figure 12(a) plots the critical ejection time T_{crit} (in milliseconds) verses the pipe flow velocity (in m/s). This data is obtained for each pipe flow velocity $U : 0.05 - 0.6$ m/s in steps of $\Delta U = 0.05$ m/s. Figure 12(b) shows

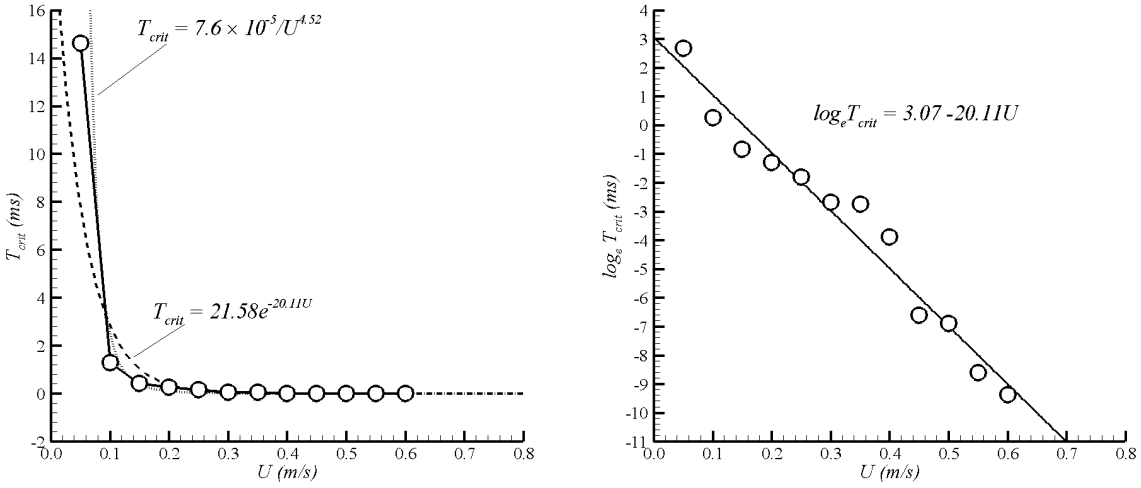

FIGURE 12. Plots of (a) critical ejection time T_{crit} as a function of pipe flow velocity U for $V_{pend} = 13$ μL and (b) the same graph with a log graph for T_{crit}.

the same plot except with the T_{crit} axis in log format. We may match the plotted data either as a power or exponential fit so that we obtain, in dimensional units T_{crit} in seconds and U in m/s:

$$T_{crit} = 21.58 \times 10^{-6} e^{-20.11U}, \qquad \text{or} \qquad T_{crit} = 7.6 \times 10^{-11} U^{-4.52} \tag{13}$$

Note that these two kinds of curve fitting only correspond with the data available, that is, with those points obtained from the simulations which do not include extreme values such as very large or very small values of U. Presently, the graph of Figure 12(a) indicates that as $U \to 0$ the critical ejection time $T_{crit} = 21.58$ ms

using equation (13)(a), this is however not defined for (13)(b). Similarly, equation (13)(a) also indicates that as $U \to \infty$ $T_{crit} = 0$ which appears to be approximately accurate as seen from Figure 12(a) although we obtain a value of $T_{crit} \simeq 0$ at about $U \simeq 0.45$ m/s after which the ejection time remains zero. To ascertain the accuracy of the current line fit it is necessary to conduct further simulations for very small values of U, for example $U : 0.001 - 0.05$ m/s and for larger values of U for example: $U : 0.7 - 1.5$ m/s.

Figure 12(b) shows the log version of the first graph which corresponds to approximately the functional form: $\ln(T_{crit}) = -20.11U + 3.07$. This shows that the graph is quite well approximated by an exponential curve. One cannot be certain that the graph will maintain a constant slope as we approach the end points for small or large velocities. To some degree the graph tends to indicate that the slope will deviate from a constant as the velocity becomes small. Strictly speaking at a zero velocity no movement takes place and the original pendant drop remains attached to the pipe. For this reason we expect the critical ejection time to tend towards infinity as $U \to 0$. In a similar sense we see from Figure 12(b) that for a velocity of approximately $U = 0.7$ m/s the critical ejection time tends to zero. What this implies is that the amount of time a flow needs to be turned on for in order to eject a drop is close to zero as the velocity approaches 0.7 m/s. This corresponds to a unit discontinuous pulse such that this pulse alone is sufficient to cause a disturbance in the stable pendant drop system to cause it to become unstable and eject a drop. In reality, the flow cannot be initiated in this way as no matter how small the amount of time a flow is turned on for it delivers a small volume of fluid. However it does provide a possible limit on the maximum pipe flow velocity for which the critical ejection time is zero.

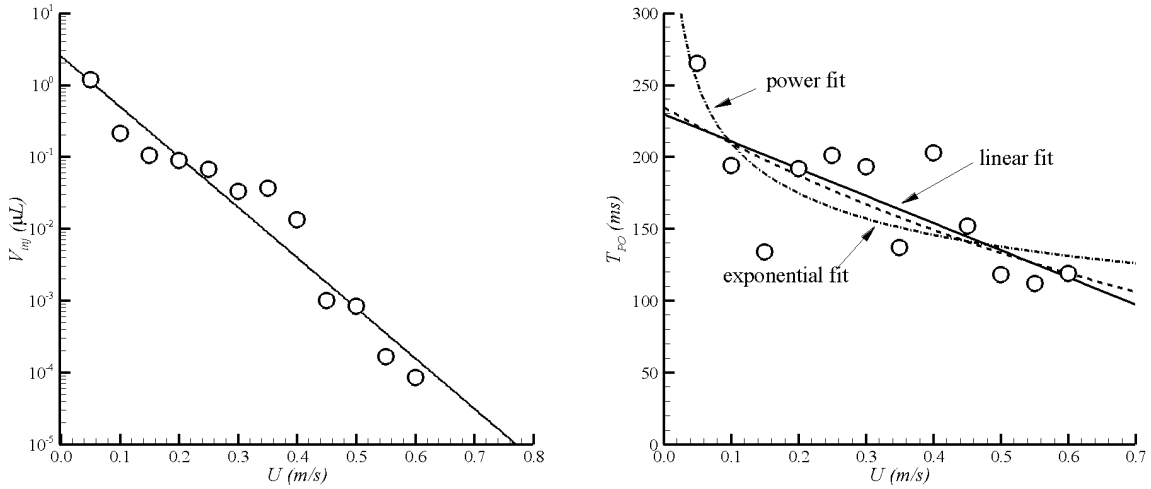

FIGURE 13. Plots of (a) critical ejection volume V_{crit} as a function of pipe flow velocity U for $V_{pend} = 13$ μL and (b) a graph showing the total time to pinch-off T_{PO} after the flow is turned off.

The critical total pendant drop volume $V_{pend} + V_{inj}$ which is given by the existing pendant drop volume and the amount injected into the pipe $V_{inj} = 21.58\pi R^2 U e^{-20.11U}$ may be written so that:

$$V_{crit} - V_{pend} = 10.79\pi R^2 U e^{-20.11U} \tag{14}$$

which corresponds to the volume shown in Figure 13(a). From the approximation (14) we see that the coefficient in the exponential -20.11 must have the units of s^{-1} and the coefficient 10.79 must have units of time. This is also true for equation (13)(a) whereas for (13)(b) the coefficent 7.6×10^{-11} must be of the functional form: $U^{4.52}t$ otherwise the units do not match.

Figure 13(b) on the other hand shows the total time needed to pinch off T_{PO} after the flow has been turned off. It is clear that this time can be very long when compared to the critical ejection time and appears to be down to an instability created within the original pendant drop system just enough to eventually eject a drop. It is not clear from the figure whether the points conform to any particular type of fit although we once again expect that as $U \to 0$ the time to pinch-off tends towards infinity as at zero velocity no fluid has been added to the pendant drop and the existing fluid has not been disturbed.

6. Mechanism of Drop Ejection

The main difference between the continuous and discrete systems has to do both with the sudden flow impulse when the flow is turned on and the discontinuous jump in velocity when the flow is turned off. From the results of Section 5 we see that these two discontinuities in flow velocity destabilise an initially stable pendant drop system so that a drop is ejected even when the total volume of the pendant drop plus the fluid added over time T_{crit} is less than the static release volume V_d.

6.1. **Flow Resistance**

It is important to understand how this instability comes about. Figure 14 shows the development of the pendant drop shape at the capillary exit at a time of $t = 0.85$ ms after the flow is turned on for two different pipe flow velocities: $U = 0.1$ and 0.6 m/s. The figure also shows the flow inside the forming pendant drop.

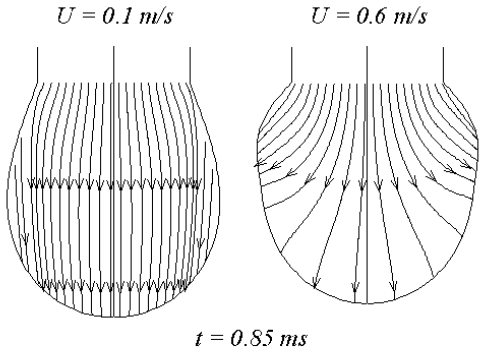

Figure 14. Streamline plots of the magnitude of velocity $|\mathbf{u}|$ of drop formation at the capillary exit for (a) $U = 0.1$ m/s (left) and (b) $U = 0.6$ m/s (right) showing streamlines within the forming drop.

The low velocity case shows almost vertically down streamlines, Figure 14(a), whereas the high velocity case shows that the streamlines have been diverted from the vertical, Figure 14(b). It is clear that, provided the pipe flow velocity is quite low, the fluid injected into the drop from the capillary suffers virtually no resistance when it flows into the existing pendant drop. However, for high pipe flow velocities the existing pendant drop fluid is unable to adjust quickly enough to the inflow and offers resistance to it. The inflowing fluid is forced sideways to either side of the pendant drop, Figure 14(b). The free surface of the pendant drop is free to move and adjusts to the sideways fluid movement by bulging outwards at the fixed end of the capillary exit.

The timescales involved show how this comes about. The advective timescales for the low and high velocity cases are: $T_{adv}^{U=0.1} = R/U = 10.2$ ms whereas $T_{adv}^{U=0.6} = 1.7$ ms respectively. The viscous timescale is given by $T_{visc} = \rho R^2/\mu = 43.6$ ms. The viscous timescale measures the time taken for a fluid to adjust to an imposed flow. We see immediately that $O(T_{adv}^{U=0.1}) \simeq O(T_{visc})$, both flow timescales are of the same order of magnitude. However, the high velocity case has $O(T_{adv}^{U=0.6}) \ll O(T_{visc})$, an order of magnitude less than the low velocity

case. This may be summarised through the corresponding Reynolds number which is a function of these two timescales: $Re = T_{visc}/T_{adv} = \rho RU/\mu$, therefore $Re^{U=0.1} = 43.6/10.2 = 4.3$ and $Re^{U=0.6} = 43.6/1.7 = 25.6$. This is a clear example of fluid inertia, the inertia of the stationery pendant drop, and can be measured by the Reynolds number for each case of imposed flow velocity.

Since surface forces always attempt to reduce surface energy a capillary wave is generated which travels along the free surface in the vertically downwards direction.

6.2. **Capillary Wave Generation**

Figure 15 shows contour plots of the magnitude of velocity inside the forming pendant drop every 0.85 ms after fluid starts to be injected into the pipe for the low and high velocity cases. Clearly, no capillary wave is generated for the low velocity case and it is used here for comparison. For the high velocity case, Figure 15(b),

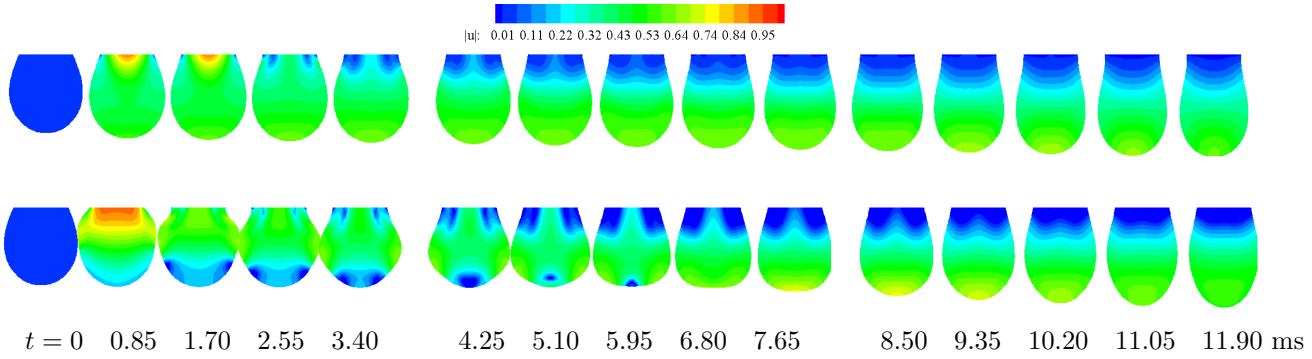

FIGURE 15. Contour plots of the magnitude of velocity $|\mathbf{u}|$ of drop formation at the capillary exit for (a) $U = 0.1$ m/s (top) and (b) $U = 0.6$ m/s (bottom) at times after the flow is turned on. (N.B. all contour plots are shown in non-dimensional form as defined in Section 4, equations (6)-(11).)

we can observe the motion of the capillary wave as it moves along the free surface of the forming pendant drop. At first, $t = 0.85$ ms, the inflowing fluid is forced sideways creating a bulge at the sides (at the capillary exit where the fluid is pinned to the pipe wall at $z = 0$, $r = R$) of the original pendant drop shape. The plot shows the high and low velocity regions inside the drop as red/orange and blue colours respectively. A high velocity region is clearly shown at the top of the forming drop (capillary exit) as the inflowing fluid attempts to enter the existing pendant drop. The flow is turned off after a very small interval, $T_{crit} \simeq 0.0001$ ms, this is shown by the sudden low velocity region at the capillary exit when $t = 1.70$ ms. Note that while the velocity at the capillary exit is still quite high $\simeq 0.36$ m/s the region at the bottom of the forming drop remains at a low velocity $\simeq 0.12$ m/s. The higher velocity region near the top of the drop is seen to move along a horizontal front vertically down the drop. At $t = 2.55$ ms it gradually approaches the bottom of the drop and the capillary wave along the free surface has also moved. In fact we see that the bulge of fluid initially at the capillary exit has moved further down along the drop and carries fluid with it. By $t = 3.40$ ms the top of the drop is now a low velocity region whereas the higher velocity region attached to the bulge of fluid on either side of the drop has now confined the low velocity region at the bottom of the drop into a small zone. At $t = 4.25$ ms this low velocity region has shrunk considerably while the bulge on either side approaches the bottom of the drop. At $t = 5.10$ ms the drop has elongated as the capillary wave has almost reached the bottom-centre of the pendant drop. The fluid on either side now converges towards the centre-bottom of the drop. By $t = 7.65$ ms the low velocity region at centre-bottom of the drop is now a higher velocity region $\simeq 0.42$ m/s. This pushes the flow further down and continues to elongate the drop thereby avoiding a tendency for the drop to oscillate in this unstable configuration. By $t = 10.20$ ms the gravitational timescale starts to take effect ($T_{grav} = \sqrt{R/g} = 10.2$

ms). This now takes over and stretches the drop vertically downwards, $t = 11.90$ ms. We see that the capillary wave, with timescale $T_{cap} = \sqrt{\rho R^3/\sigma} = 5.0$ ms has completed its motion between the times of $t : 1.70 - 8.50$ ms.

We may compare this with the low velocity case and see immediately that at each time the inflowing fluid has been able to penetrate into the existing pendant drop with low resistance. This is why there are no low velocity regions at the bottom of the drop as was seen in the high velocity case. The characteristic flow is quite different although the end result reached at $t = 11.90$ ms is similar. The instability which generated the capillary wave for large pipe flow velocities is large enough to induce drop ejection even for extremely small amounts of fluid injected into the pipe, see Figures 12 and 13. The capillary wave shows how fluid is transported from the neck region near the capillary exit to the bottom of the drop.

6.2.1. *Minimum Neck Radius-Limiting Length Aspect Ratios*

Two other measures of drop formation characteristics are: (i) the limiting length L_d which measures the length between the capillary exit, $z = 0$ in Figure 7, and the lowest point on the free surface along the symmetry axis ($r = 0$) of the forming drop and (ii) the minimum neck radius r_{min} which measures the minimum distance in the radial direction between the symmetry axis and the closest point on the free surface. These two measures

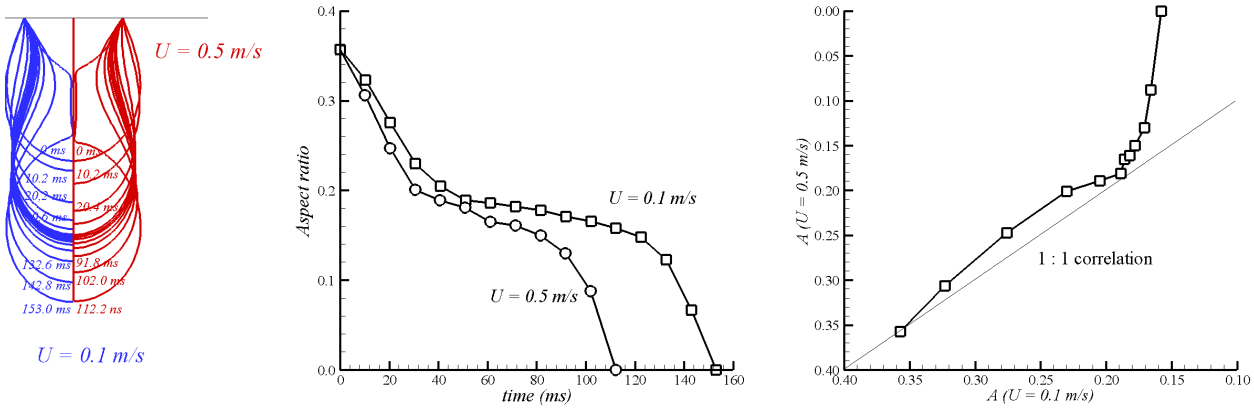

FIGURE 16. Plots of (a) free boundaries for the $U = 0.1$ m/s and 0.5 m/s cases showing times after flow initiation (b) time verses aspect ratio for the $U = 0.1$ m/s and $U = 0.5$ m/s cases and (c) a direct comparison between the two aspect ratios.

may be used to construct an aspect ratio $A = r_{min}/L_d$ which measures how quickly the minimum neck radius decreases with respect to the limiting length before pinch-off occurs. This is shown in Figure 16(b) for the case of $U = 0.1$ m/s and 0.5 m/s. In Figure 16(a) is shown the shape of the forming drop on either side of the symmetry axis starting at $t = 0$, when the flow is turned on, until a time where the drop pinches off for $U = 0.1$ m/s (blue) on the left hand side and for $U = 0.5$ m/s (red) on the right hand side. Although the eventual pinch-off point (as measured along the symmetry axis) appears to be virtually at the same distance from the capillary exit we see that the $U = 0.5$ m/s case pinches off at a much earlier stage than the $U = 0.1$ m/s case, at $t = 112.2$ ms compared to $t = 153.0$ ms respectively.

Figure 16(b) shows how the aspect ratio changes over time for the high and low velocity cases. At pinch-off the minimum neck radius becomes zero so that the aspect ratio is zero there. We see that the aspect ratio for both the high and low velocity cases decreases linearly at the start with almost equal slope. This is followed by a slowing down of the decrease to an inflection point followed by a rapid downturn of high negative slope. Zero aspect ratio is reached at an earlier time for the high velocity case. This implies (for the high velocity case) that fluid has been extracted from the region near the capillary exit, the necking region, and transported

to the lower part of the forming drop. This is achieved by the capillary wave which naturally travels along the free surface and takes with it the fluid encased by the "bulge" formed initially.

In Figure 16(c) we see a direct comparison between the two aspect ratios taken at the same time showing a decreasing aspect ratio left-to-right, bottom-to-top. A direct one to one correlation would indicate the straight line drawn in the figure. At first this seems to be the case with an almost linear decrease although the high velocity case still decreases faster than the low velocity case. After a brief period during which the rate of decrease slows down there is a sudden increase in the rate of decrease for the high velocity case reaching zero aspect ratio at the top of the graph while the low velocity case has still to reach this point.

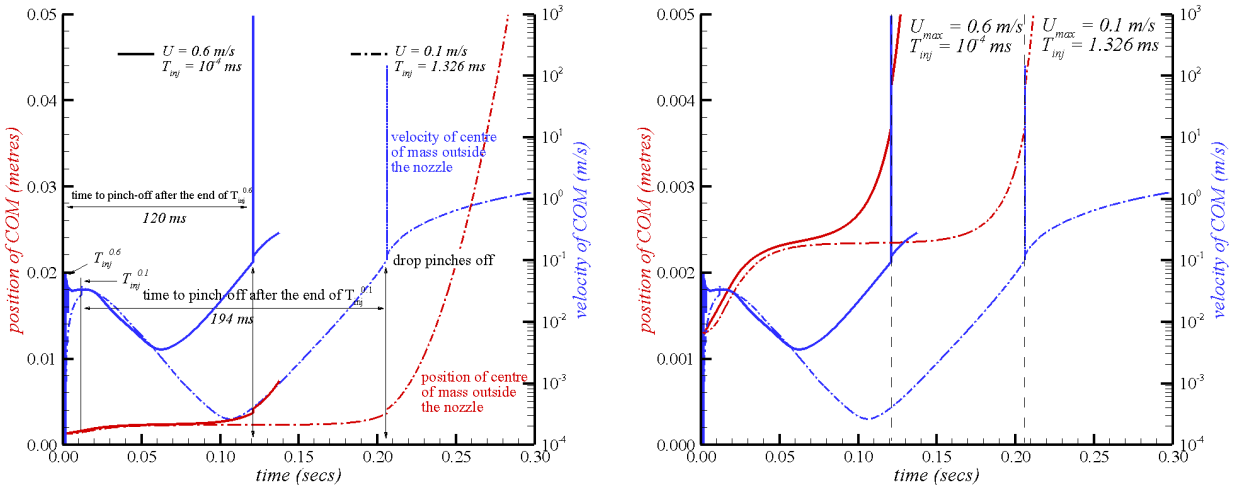

FIGURE 17. Plot showing (a) the change in the position and velocity of the centre-of-mass of the pendant drop with time and (b) a closeup of the region just before pinch-off

Figure 17 shows the change in the position and velocity of the centre-of-mass (COM) of the pendant drop for the low $U = 0.1$ m/s and high $U = 0.6$ m/s velocity cases. It is clear from Figure 17(b) that the high velocity case has a lower COM at the same time, especially after $t = 0.08$ s, as compared to the low velocity case. While the characteristic shape of the position of the COM is the same in both cases the low velocity case spends a good deal more time in a period where its position changes very little: $\Delta t \simeq 0.07$s for the low velocity case as compared to $\Delta t \simeq 0.01$.

7. CONCLUSIONS

This paper has investigated critical drop formation and ejection behaviour for discrete pipe flow from a capillary. It is clear that for an initial pendant drop volume of $V_{pend} = 13$ μL:

(1) There is a distinct difference between the continuous and discrete flows from a capillary. This difference occurs because the discrete pipe flow is delivered in a discontinuous step-wise fashion. From the results shown in this paper it is clear that the two flow discontinuities at initiation and cessation of the discrete flow are the cause of the difference in drop formation behaviour between the discrete and continuous cases.

(2) We have shown that the critical time needed to inject fluid into the pipe in order to just eject a drop depends on the pipe flow velocity and may be written as an exponential in the following form: $T_{crit} = C_0 e^{-\alpha U}$ where $C_0 = 21.58 \times 10^{-6}$s and $\alpha = 20.11$ m^{-1}s. Similarly, there is a corresponding critical volume required to eject a drop given by $V_{crit} = V_{pend} + \pi R^2 U T_{crit}/2$.

(3) For larger flow velocities, an impulsive velocity discontinuity at the initiation of the discrete flow at the capillary exit, and inertial flow resistance of the existing pendant drop, forces fluid to either side of the capillary exit rather than vertically downwards. The free surface pinned to the capillary exit bulges outward on either side of the exit. This creates a capillary instability and gives rise to a capillary wave which travels down the free surface transporting fluid along with it.
(4) As the capillary wave transports fluid from the upper right and left sides of the pendant drop at the capillary exit it removes fluid from this region. This creates a thinning of the neck region joining the capillary exit with the lower part of the pendant drop and consequently an enlargement of the lower part of the pendant drop.
(5) We have shown that for large pipe flow velocities a drop is ejected at an earlier time than for low pipe flow velocities. The data has shown that the centre of mass of the pendant drop is lower for the high velocity case and that drop aspect ratios decrease to zero faster than for the low velocity cases.

This is a preliminary study and requires further work such as experimental support. In addition, the results of this paper have studied the single case of an existing pendant drop volume of $V_{pend} = 13$ μL and other cases involving much lower values of V_{pend} should be investigated. For such low pendant drop volumes, e.g. $V_{pend} = 5$ μL, a good deal more fluid must be injected into the pipe in order to eject a drop. This means that the injection time needed to eject a drop is longer and that fluid continues to flow into the existing pendant drop for longer periods of time while a capillary wave is still expected to be generated at high pipe flow velocities. Such a study would require an extra flow parameter such as the injection volume in addition to the pipe flow velocity used in this paper. It also requires an answer to the question of how much drop ejection is affected by a longer fluid injection time as compared to the capillary wave explanation described here. Further numerical experiments could also be done to study how the the current results are affected by a change in fluid parameters so that it may become possible to be able to express discrete drop formation in terms of dimensionless operability diagrams akin to those already constructed for the continuous case [1].

References

[1] Subramani H.J., Yeoh H.-K., Suryo R., Xu Q., Ambravaneswaran B., Basaran O. Simplicity and Complexity in a Dripping Faucet. Phys. Fluids, 18:032106-1032106-13, 2006.
[2] Bogy, D.B Drop Formation in a Circular Liquid Jet. Ann. Rev. Fluid Mech., 11:207–228, 1979.
[3] Eggers, J. Nonlinear Dynamics and Breakup of Free-Surface Flows. Rev. Modern Phys., 69(3):865–929, 1997.
[4] Lin. S.P., Reitz, R.D. Drop and Spray Formation from a Liquid Jet. Ann. Rev. Fluid Mech., 30:85-105, 1998.
[5] Henderson, D.M., Pritchard, W.G., Smolka, L. On the Pinch-Off of a Pendant Drop of Viscous Fluid. Phys. Fluids, 9(11):3188–3200, 1997.
[6] Zhang, X., Basaran, O.A. An Experimental Study of Dynamics of Drop Formation. Phys. Fluids, 7(6):1184–1203, 1995.
[7] Cramer, C., Studer, S., Windhab, E.J., Fischer, P. Periodic Dripping Dynamics in a Co-Flowing Liquid-Liquid System. Phys. Fluids, 24:093101, 2012.
[8] Clasen, C., Phillips, P.M., Palangetic, L., Vermant, J. Dispensing of Rheologically Complex Fluids: The Map of Misery. AIChE J., 58(10):3242–3255, 2012.
[9] Harkins W.D., Brown F.E. The Determination of Surface Tension (Free Surface Energy), and the Weight of Falling Drops: The Surface Tension of Water and Benzene by the Capillary Height Method. J. Am. Chem. Soc, 41:499–524, 1919.
[10] Dong, H., Carr, W.W., Morris, J.F. An Experimental Study of Drop-On-Demand Drop Formation. Phys. Fluids, 18:072102, 2006.
[11] Xu, Q., Basaran, O.A. Computational Analysis of Drop-On-Demand Drop Formation. Phys. Fluids, 19:102111, 2007.
[12] Derby, B. Inkjet Printing of Functional and Structural Materials: Fluid Property Requirements, Feature Stability, and Resolution. Ann. Rev. Mater. Res. 40:395–414, 2010.
[13] Peregrine, D.H., Shoker, G., Symon, A. The Bifurcation of Liquid Bridges. J. Fluid Mech., 212:25–39, 1990.
[14] Harlen, O.G., Rallison, J.M., Szabo, P. A Split Lagrangian-Eulerian Method for Simulating Transient Viscoelastic Flows. J. non-Newtonian Fluid. Mech., 60:81–104, 1995.
[15] Castrejón-Pita, J.R., Morrison, N.F., Harlen, O.G., Martin, G.D., Hutchings, I.M. Experimental and Lagrangian Simulations on the Formation of Droplets in Continuous Mode. Phys. Rev. E, 83:016301-1–016301-10, 2011.
[16] Castrejón-Pita, J.R., Morrison, N.F., Harlen, O.G., Martin, G.D., Hutchings, I.M. Experimental and Lagrangian Simulations on the Formation of Droplets in Drop-on-Demand Mode. Phys. Rev. E, 83:036306-1–036306-12, 2011.
[17] Clanet, C., Lasheras, J.C. Transition from Dripping to Jetting. J. Fluid. Mech., 383:307–326, 1999.